Variational Transition-State Theory Study of the Dimethyl Sulfoxide (DMSO) and OH Reaction†

Núria González-García, Àngels González-Lafont,* and José M. Lluch

Departament de Química, Universitat Autònoma de Barcelona, 08193 Bellaterra (Barcelona), Spain

Received: August 8, 2005; In Final Form: October 11, 2005

The mechanism for the atmospheric oxidation of DMSO has been studied. For the first time, all the possible channels in the DMSO + OH reaction are studied together theoretically, and their corresponding rate constants have been evaluated under the variational transition-state formalism. Three different channels have been characterized: an addition−elimination process to form MSIA (CH_3SOOH) and CH_3, a H-abstraction pathway to give CH_3SOCH_2 and H_2O, and a nonkinetically relevant S_N2-type reaction to form methanol and CH_3SO. In agreement with previous experimental and theoretical works, the main product in the DMSO + OH reaction turns out to be the MSIA, with a branching ratio at 298.15 K around 97%. The effects of pressure in the global rate constant have also been analyzed.

1. Introduction

Dimethyl sulfoxide (DMSO) is considered to be an important intermediate in the atmospheric oxidation of dimethyl sulfide (DMS). It has been identified in both laboratory[1−5] and field studies.[6−8] Although it is an important DMS oxidation secondary product, its reactions in the atmosphere have received little attention. DMS, emitted from phytoplankton in the oceans, is the major natural source of sulfur in the atmosphere. DMS accounts for 10−40% of the total sulfur emitted to the atmosphere, equivalent to 12−54 Tg S/year.[9−11] It has been proposed that DMS could be a major source of sulfate aerosols over the oceans. In addition to the direct radiative impact of these aerosols, they may also have an impact on the number of available cloud condensation nuclei (CCN) which, in turn, can influence the albedo of clouds over the oceans. Thus, it has been postulated that the emission of DMS from the oceans may have a significant influence on the Earth's radiation budget and possibly interacts with climate change.[12]

The production of DMSO in the hydroxyl radical-initiated oxidation of DMS is thought to involve two steps: first, the addition of the OH radical to the sulfur atom of DMS to form a stable adduct, followed by the reaction of this adduct with molecular oxygen.[4,13,14] Although different DMSO yields for this reaction have been published,[4,5,14] all the studies confirm that DMSO formation is quite substantial. However, the absolute yield of DMSO under atmospheric conditions is still uncertain. It has been proposed that the reaction of DMS with BrO radicals could contribute to the fate of DMSO in the atmosphere, too.[15−17] The reaction of OH with DMSO has been found to be very fast, so this removal process is likely to be the dominant atmospheric sink of DMSO. For instance, at room temperature and atmospheric pressure, the OH-initiated oxidation of DMSO is approximately 15 times faster than the reaction of OH with DMS: $k_{DMSO+OH} = 9.4 \times 10^{-11}$ cm^3 molecule^{-1} s^{-1} [18] compared to $k_{DMS+OH} = 6.5 \times 10^{-12}$ cm^3 molecule^{-1} s^{-1}.[19] Several experimental studies have investigated the hydroxyl radical-initiated oxidation of DMSO. There is general agreement that the products observed in smog chamber studies are sulfur dioxide (SO_2), dimethyl sulfone ($DMSO_2$, $CH_3S(O)_2CH_3$), methane sulfinic acid (MSIA, $CH_3S(O)OH$), methane sulfonic acid (MSA, $CH_3S(O)_2OH$), and methanesulfonyl peroxynitrate (MSPN, $CH_3S(O)_2OONO_2$).[3,20] However, the reported product yields differ significantly depending on the experiment. Barnes et al.[20] observed significant amounts of SO_2 but lesser amounts of $DMSO_2$ by performing an FTIR study. Contrarily, Sørensen et al.[3] reported production of SO_2 and $DMSO_2$ in almost equal amounts. They could not observe formation of MSIA and reported an upper limit for MSIA yield of 0.3%. In contrast, Urbanski et al.[21] concluded that the CH_3 yield from the OH-initiated oxidation of DMSO was 0.98 ± 0.12 in the absence of O_2. Since, according to those authors, MSIA was the principal coproduct of methyl radical in the OH + DMSO reaction, a near-unity yield was also proposed for MSIA. All the experiments carried out so far for the DMSO + OH reaction propose the two following pathways in the absence of O_2:

$$CH_3S(O)CH_3 + OH \rightarrow [CH_3S(O)(OH)CH_3] \rightarrow CH_3S(O)OH + CH_3 \quad (R1)$$

$$CH_3S(O)CH_3 + OH \rightarrow CH_3S(O)CH_2 + H_2O \quad (R2)$$

Some important mechanistic information has also been published. Hynes and Wine[18] found the rate coefficient for DMSO + OH reaction to be indepenent of the pressure (25−700 Torr); no isotope effect was measured by using the deuterated DMSO, and no evidence of reversible adduct formation was observed. Those findings are consistent with OH addition to DMSO to form an adduct that does not decompose back to reactants on the time scale of their observations and with the H-abstraction channel being of minor importance in the DMSO + OH reaction. The findings of Hynes and Wine were confirmed by Urbanski et al.[21] who stablished that, if a stabilized $CH_3S(O)(OH)CH_3$ adduct is formed, its lifetime toward decomposition is less than 10 μs at 20 Torr and 298 K. Their reported room-temperature rate coefficient for the OH + DMSO reaction is $(8.7 \pm 1.6) \times 10^{-11}$ cm^3 molecule^{-1} s^{-1}. The most recent studies have concentrated their interest on this reaction in MSIA formation.[22,23] Arsene et al.[22] studied the product formation in

† Part of the special issue "Donald G. Truhlar Festschrift".

10.1021/jp054424x CCC: $33.50
Published on Web 12/03/2005

both the absence and the presence of NO_x. They used a total pressure of 1000 mbar of synthetic air at 284 ± 2 K. The evolution of reactants and products were monitored in situ using FTIR spectroscopy. For MSIA and MSA detection, the ion chromatography (IC) analytical tool was employed. The measured yields of MSIA were very high (84−99%), although the same authors indicate that MSIA quantification was difficult and is only semiquantitative in their study. Stable secondary products in the system were very scarce: SO_2, $DMSO_2$, MSA, and MSPN accounted for only about 15% and 12% of sulfur in the presence and absence of NO_x, respectively. In addition, the formation of MSA is, according to Arsene et al.,[22] clear evidence that this compound can also be formed via the addition channel of the OH radical-initiated oxidation of DMS. Kukui et al.[23] used a high-pressure turbulent flow reactor coupled to an ion molecule reaction mass spectrometer to study the reactions of OH radical with DMSO and MSIA at 298 K and 200 and 400 Torr of N_2. These measurements seem to be the first direct detection of MSIA in the OH + DMSO gas-phase reaction, and the estimated yield of this compound was 0.9 ± 0.2. The reaction rate constant reported by the authors is $(9.0 \pm 1.6) \times 10^{-11}$ cm^3 molecule^{-1} s^{-1}, in very good agreement with previous experimental results. As for the reaction between MSIA and OH radical, they concluded that SO_2 is the major product of this oxidation process. Their results then indicate that the OH-addition route of the gas-phase atmospheric oxidation of DMS, which produces DMSO, would result in high yields of SO_2, which is a precursor of H_2SO_4. Another interesting conclusion of their work is that MSA, the other major end product of DMS oxidation, is not produced by gas-phase reactions involving MSIA, as have been suggested before.

To our knowledge, only two theoretical works on the reaction of DMSO with OH have been published.[24,25] Wang and Zhang[24] reported ab initio studies on the stationary points involved in this reaction. Two addition complexes and three different saddle-point structures at the MP2/6-311G(d,p) level of theory were characterized. As had been experimentally suggested, they found an addition complex ($(CH_3)_2S(O)OH$ interaction) that could further undergo decomposition to form MSIA and CH_3 (R1). The other complex found ($(CH_3)_2SO-HO$ interaction) was not linked to the abstraction channel (R2), although their connection was suggested. Finally, a third saddle point was characterized as corresponding to the S_N2-type reaction leading to CH_3OH + CH_3SO (R3). Their best estimation of the energetics corresponded to the G3//MP2/6-311G(d,p) level of theory. On the

$$CH_3S(O)CH_3 + OH \rightarrow CH_3SO + CH_3OH \qquad (R3)$$

other hand, Resende et al.[25] concentrated their efforts on the study of the role of adducts along the DMSO + OH path in the DMSO atmospheric oxidation. They found the same two addition complexes as Wang and Zhang[24] and a third one very similar to the $(CH_3)_2SO-HO$ structure but with the hydroxyl radical oxygen atom closer to one of the hydrogens in DMSO. The authors linked this nonsymmetric hydrogen-bonded complex with the unique saddle-point structure found for the abstraction channel (R2). In agreement with Wang and Zhang, the $(CH_3)_2S(O)(OH)$ complex was connected with the CH_3 elimination saddle-point structure (R1). The final energetics was calculated at the CCSD(T)/cc-pVTZ//UMP2/6-31G(d) level. Also in agreement with previous results, the calculations of Resende et al.[25] give a lower free energy barrier for the elimination channel than for the abstraction pathway. A common free energy bottleneck estimated by simple collision theory was assigned by the authors to the formation of the two weakly bound complexes. Within the framework of conventional transition-state theory and using the steady-state approximation for the two complexes, the authors calculated a global rate constant of 1.44×10^{-10} cm^3 molecule^{-1} s^{-1} at 298 K, slightly greater than the experimental upper limit.

The standard steady-state analysis carried out at the canonical ensemble by Resende et al.[25] presumes that the two weakly bound complexes have thermal distribution of states. This thermal distribution would only arise if the complexes suffer many collisions before reacting, that is, at the high-pressure regime. However, under experimental conditions, no indication of stabilized complex formation was found, or at least, most of the authors who carried out those experiments stress their doubts about the existence of a thermalized adduct corresponding to the addition−elimination channel. Herein, a kinetic study within the framework of variational transition-state theory of the OH-initiated oxidation of DMSO was carried out at the two limiting pressure regimes. At low pressure, the canonical unified statistical theory[26] was used to calculate the global rate constants, whereas at high enough pressure, the calculation of the canonical global rate constant was carried out within the steady-state approximation. The comparison of the two rate constant values will allow us to infer whether pressure effects might be important in the OH-initiated degradation of DMSO.

2. Method of Calculation

In this section, we will describe the technical details of the electronic structure and the dynamical calculations.

2.1. Electronic Structure Calculations. Geometry optimization, energies, and first and second energy derivatives for the three reactions were calculated by using two different electronic structure approaches: second-order Møller−Plesset perturbation theory (MP2)[27] and hybrid density functional theory (HDFT).[28−31] At the HDFT level, three different hybrid functionals were tested: MPW1K[32] (modified Perdew−Wang one-parameter model for kinetics), BB1K[33] (Becke88−Becke95 one-parameter model for kinetics), and MPWB1K[34] (modified Perdew and Wang 1991 exchange functional[35] and Becke's 1995 meta correlation functional).[36] This last HDFT method is actually a hybrid meta DFT[37] (HMDFT), because it depends on kinetic energy density as well as the density and the gradient of the density. All these HDFT methods have been tested against kinetic databases. They have also shown a good compromise between cost and accuracy in describing heavy atom transfer reactions.[38] The HDFT results are compared to MP2 theory calculations, which have also been used in previous works to study the thermodynamics of this system.[24,25] We used spin-projected MP2 energies (PMP2)[39] to correct for spin contamination effects, even though the value of $\langle S^2 \rangle$ was never higher than 0.82. Two different sets of basis functions have been employed: the 6-31+G(d,p) Pople basis set[40] and the MG3S basis set[41] from Truhlar's group. The MG3S basis set[41] is identical to 6-311++G(2df,2p) for C, O, and H, except that, on hydrogen, diffuse functions have been removed. For the sulfur atom, this basis set stands for the 6-311+G(3d2f) Pople's one. The most important factor in choosing the MG3S basis is that it includes tight d functions that seem to be a prerequisite for consistent accuracy on second-row atoms. The MG3S satisfies this criterion, because the exponent of the tighest d function for *S* is 2.6.[42] Energies at all the stationary points were then recalculated at a higher level of theory, the multicoefficient Gaussian-3 method, in its version 3s (MCG3/3).[43,44] This approach has been proven to represent a very good compromise of accuracy, cost, and ease of use for practical calculations in

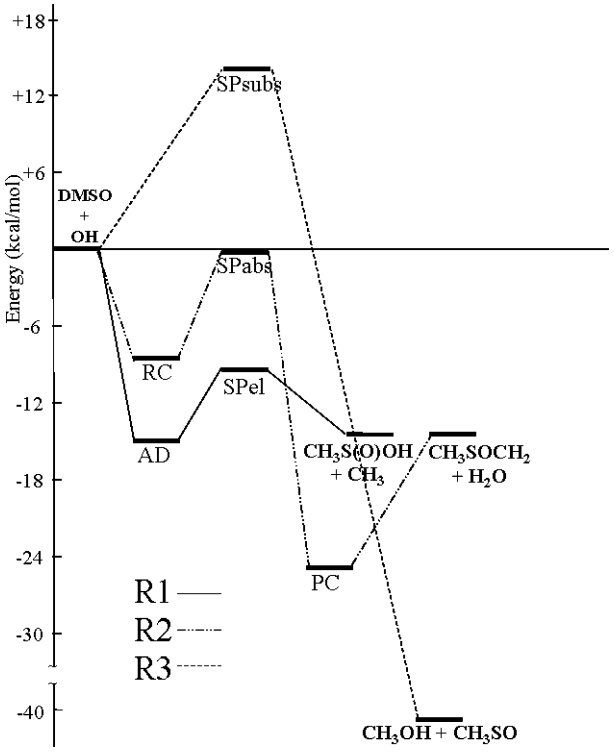

Figure 1. Classical potential energy diagram for the DMSO + OH reaction: three reaction channels are shown. Energies calculated at the MCG3/3//MPW1K/MG3S level.

thermochemical kinetics. Core correlation effects are implicitly included in the parametrization. The main advantage of the MCG3 method, and, in general, of multicoefficient methods, is that they can be used to calculate potential energy surfaces (PESs), because the energy expression is a continuous function of the geometry because of the elimination of the high-level correction (HLC) term[43,44] included in other methods. The nature of the stationary points has been determined by means of the analysis of the number of imaginary frequencies: NIMAG = 1 for saddle points, or NIMAG = 0 for minima. The different stationary points found correspond to the three reaction mechanisms mentioned in the Introduction section: an addition−elimination channel (R1), a H-abstraction channel (R2), and an S_N2 pathway (R3). The two mechanisms R1 and R2 were found to proceed via a complex in the entrance channel. In R1, an addition-type of complex (which will be called AD) is formed, and then, it is followed by the elimination of a methyl group to form MSIA. The methyl elimination takes place through a saddle-point structure (SP_{el}). In R2, a H-bonded-type of complex (which will be called RC) is formed first, followed in this case by the saddle-point structure of the H-abstraction process (SP_{abs}). Also, for the H-abstraction channel, a complex was found at the product side of the reaction (PC). In contrast, in the R3 channel, a unique stationary point was located corresponding to the nucleophilic-substitution saddle-point structure (SP_{subs}). A global description of the three degradation routes for the DMSO + OH reaction is depicted in Figure 1.

To ensure the connectivity between the stationary points found and for their use in the dynamical calculations, the minimum energy path (MEP)[45] in an isoinertial mass-weighted Cartesian coordinate system was calculated starting from each saddle-point geometry found (SP_{el}, SP_{abs}, and SP_{subs}), by following the Page−McIver algorithm[46] at the MPW1K/MG3S level of theory. A step size, δs, of 0.01 bohr (where s denotes the distance along the MEP in an isoinertial mass-scaled coordinate system with a scaling mass equal to 1 amu) was used in all cases. The second derivative matrix was calculated at every two points on each MEP. For all the regions, the interpolated single-point energy correction (ISPE)[47] procedure was used for the variational transition-state calculations. The ISPE method is a dual-level direct dynamics scheme that uses a low-level (LL) MEP and corrects the energy by interpolating the energy differences at some points along the MEP between this low-level MEP and single-point energy calculations at a higher level (HL). In this work, we used the MPW1K/MG3S method as the LL and the MCG3/3 as the HL. Thus, in addition to the stationary points, we calculated the HL energy at several nonstationary points along the MEPs. Because of the change of the electronic calculation level, in general, the HL classical energy maximum structure (with energy V_{max}) along the LL MEP will not coincide with the LL saddle-point structure. The normal-mode analysis along the MEP was performed in Cartesian coordinates, and the reoriented dividing surface (RODS)[48] algorithm was used to improve the generalized frequencies. For the addition and association regions (AD and RC formation, respectively), we built a distinguished reaction coordinate path (DCP) at the MPW1K/MG3S level. Since the MEP was not calculated for these regions, the use of the RODS algorithm[48] becomes necessary in order to obtain reliable generalized eigenvectors and frequencies along the DCP path. Geometry optimization and the Hessian matrix calculation for stationary points, as well as the DCPs, were carried out with the *Gaussian 03* package of programs.[49] All the single-point MCG3/3 multilevel energy calculations were performed with the *MultiLevel 4.0* code.[50] The *GaussRate 9.1* code,[51] which is an interface linking *PolyRate 9.3*[52] and *Gaussian 03*,[49] was used for calculating the LL information along the MEPs.

2.2. Dynamical Calculations. As indicated before, the reaction between DMSO and hydroxyl radical can proceed via three different pathways. They are therefore three competitive reactions. To obtain the global reaction rate constant at the low-pressure regime, we applied the competitive canonical unified statistical (CCUS) theory,[53] in which the global reaction rate constant, $k^{CCUS}(T)$, is given by

$$k^{CCUS}(T) = k_{R1}(T) + k_{R2}(T) + k_{R3}(T) \quad (1)$$

where $k_{R1}(T)$, $k_{R2}(T)$, and $k_{R3}(T)$ are the rate constants for the addition−elimination, abstraction, and S_N2 mechanisms, respectively. When several complexes are formed along a mechanism, there can be several bottlenecks in that pathway. Actually, there could be one at every region in each individual channel. This is the situation for channels R1 and R2. Then, the canonical unified statistical (CUS) theory[26] must be applied, and the corresponding rate constants for each channel will be given by

$$\frac{1}{k_{R1}(T)} = \frac{1}{k_{add}(T)} - \frac{1}{k_{AD}(T)} + \frac{1}{k_{el}(T)} \quad (2)$$

$$\frac{1}{k_{R2}(T)} = \frac{1}{k_{ass}(T)} - \frac{1}{k_{RC}(T)} + \frac{1}{k_{abs}(T)} - \frac{1}{k_{PC}(T)} + \frac{1}{k_{diss}(T)} \quad (3)$$

where $k_{AD}(T)$, $k_{RC}(T)$, and $k_{PC}(T)$ are the one-way flux rate constants evaluated at the complexes formed along the reactions paths. The $k_{add}(T)$, $k_{el}(T)$, $k_{ass}(T)$, $k_{abs}(T)$, and $k_{diss}(T)$ are the rate constants for the addition, elimination, association, abstraction, and dissociation regions, respectively, calculated at the corresponding bottlenecks. However, the dissociation region was not included in the final $k_{R2}(T)$ evaluation because of the high exothermicity of the channel: $k_{PC}(T)$ and $k_{diss}(T)$ take very high

values, and their contribution to the global R2 flux becomes irrelevant. Note that, despite the separation in different regions that we have done for each mechanism, according to the CUS theory[26] all the rate constants are calculated with the same reactants, DMSO and OH. The rate constant expression for channel R3, $k_{R3}(T)$, is given by the only bottleneck found along the pathway, which is the one corresponding to the saddle point of the reaction; then

$$k_{R3}(T) = k_{SPsubs}(T) \tag{4}$$

At the high-pressure regime, the global rate constant was calculated according to eq 5 where it is assumed that the AD complex of the R1 channel and the RC complex of the R2 channel present a thermal distribution of their corresponding energetic states.

$$k^{High-P}(T) = k_{R1}(T) + k_{R2}(T) + k_{R3}(T) \tag{5}$$

The steady-state approximation was then used for these two species in order to obtain the one-way flux rate constants for R1 and R2 (see eqs 6 and 7) channels

$$k_{R1}(T) = \frac{k_{add}(T)k_{el}^{High-P}(T)}{k_{-add}(T) + k_{el}^{High-P}(T)} \tag{6}$$

$$k_{R2}(T) = \frac{k_{ass}(T)k_{abs}^{High-P}(T)}{k_{-ass}(T) + k_{abs}^{High-P}(T)} \tag{7}$$

Note that $k_{el}^{High-P}(T)$ and $k_{abs}^{High-P}(T)$ refer to the elimination and abstraction rate constants, respectively, but with AD and RC complexes taken as reactants, in each case. $k_{-add}(T)$ and $k_{-ass}(T)$ refer to the inverse rate constants for the addition and association processes. $k_{add}(T)$ and $k_{ass}(T)$ are the same rate constants included in eqs 2 and 3, respectively. The $k_{R3}(T)$ rate constant is the same as in eq 4. All the rate constants were calculated by means of canonical variational transition-state (CVT) theory[54−58] and corrected with the multidimensional small-curvature tunneling (SCT) coefficient[59−62] when quantum effects on the nuclear motion where possible (i.e., when the reaction has a positive adiabatic ground-state potential energy barrier, V^{AG}, somewhere along the reaction path). The adiabatic potential energy includes classical potential energy and zero-point energy contributions. The CVT/SCT rate constant is defined as

$$k^{CVT/SCT}(T, s^*) = \kappa^{SCT}(T)\sigma\frac{k_B T}{h}\frac{Q^{GT}(T, s^*)}{Q^R(T)}\exp[-V(s^*)/k_B T] \tag{8}$$

where $\kappa^{SCT}(T)$ is the SCT transmission coefficient, s^* is the value of s at the free energy maximum along the reaction path (MEP or DCP) at temperature T, σ is the symmetry number, k_B is the Boltzmann's constant, h is the Planck's constant, $V(s^*)$ is the classical potential energy at s^* with the zero of energy at the overall classical energy of reactants, $Q^R(T)$ is the reactant partition function per unit volume (again with the zero of energy at the reactants), and $Q^{GT}(T, s^*)$ is the generalized transition-state partition function with the zero of energy at $V(s^*)$ and excluding the reaction coordinate. It should be noted that rotational symmetry numbers were removed for all partition functions, as they are included in σ. This symmetry number is calculated according to the following expression:[63]

$$\sigma(s) = \frac{n\sigma^R}{\sigma^{GT}(s)} \tag{9}$$

where n stands for the number of kinetically equivalent transition states, σ^R is the usual rotational symmetry number for reactants (or the product of these symmetry numbers if there are two molecular reactans, as in our case), and $\sigma^{GT}(s)$ corresponds to the usual rotational symmetry number of the generalized transition state at s. In our applications, we assume $\sigma^{GT}(s)$ to be independent of s, and thus, $\sigma(s)$ becomes a constant σ. In all cases, the vibrational partition functions have been evaluated within the harmonic approximation.

The ISPE algorithm was used to compute a high-level (HL) rate constant for those regions with a saddle point. The ISPE method is based on a mapping function[64] to interpolate the information along the MEP (or DCP). For the association region (barrierless reaction; i.e., without saddlepoint), a three-point Lagrange interpolation was used. All rate constants where computed with the *PolyRate 9.3* code.[52]

3. Results and Discussion

In this section, we will first present the electronic structure results of the stationary points found for the DMSO + OH reaction. After that, we will describe the reaction pathway and the kinetics results for each individual channel. Finally, the contribution of each channel to the global mechanism and the overall rate constant of the DMSO + OH reaction will be analyzed.

3.1. Stationary Points. In Table 1, a comparison of the energetics obtained at different levels of electronic structure theory for the addition−elimination, abstraction, and S_N2 channels is given. The figures in Table 1 for the addition−elimination channel indicate that MPW1K (the hybrid density functional finally selected as the low level in the electronic structure calculations of this study) tends to underestimate somewhat the stability of the AD complex when compared with the other hybrid functionals and also with PMP2 calculations. This is also the trend in the energetics at SP_{el} and in the classical potential energy for the R1 products. In any case, those energetic differences disappear when high-level corrections are introduced at the MCG3/3 level. As for the abstraction channel, the figures in Table 1 do not show any significant differences concerning RC stability using HDFT, MP2 theory, or at the MCG3/3 level, besides the fact that this entrance-channel complex was not found on the BB1K/MG3S PES. The MPW1K barrier at SP_{abs} is around 1 kcal/mol higher than that using the other two hybrid functionals, but 1 kcal/mol lower than the PMP2 result. MP2 theory clearly gives higher barriers. Those energetic differences significantly disappear at the MCG3/3 level. As for the classical potential energy for the abstraction products, one can also observe the good agreement at the MCG3/3 level, although the differences between HDFT and MP2 theories are 3−4 kcal/mol. Concerning the S_N2 channel, it is noticeable that MP2 gives very high barriers without spin contamination problems in that reaction pathway. Also, for the energetic results of this channel, the convergence at the MCG3/3 level is remarkable. By taking into account the energetic results presented in Table 1 for the DMSO + OH reaction and in order to carry out direct comparison with our previous study on the DMS + OH process,[65] the MCG3/3//MPW1K/MG3S level was finally selected as the electronic structure level of theory in this kinetic study of OH-initiated oxidation of DMSO. The optimized geometries of the minimum-energy and saddle-point structures calculated at the MPW1K/MG3S level are shown in Figure 2, while the potential energy diagram obtained at the MCG3/3//MPW1K/MG3S level was already presented in Figure 1.

TABLE 1: Energies (in kcal/mol) of the Stationary Points for DMSO + OH Reaction[a]

	reaction 1					reaction 2							reaction 3		
	V_{AD}	$(V_a^G)_{AD}$	$V_{el}^{\ddagger}$	$(V_a^G)_{el}^{\ddagger}$	ΔV_{el}	V_{RC}	$(V_a^G)_{RC}$	$V_{abs}^{\ddagger}$	$(V_a^G)_{abs}^{\ddagger}$	V_{PC}	$(V_a^G)_{PC}$	ΔV_{abs}	$V_{subs}^{\ddagger}$	$(V_a^G)_{subs}^{\ddagger}$	ΔV_{subs}
MPW1K/MG3S	−10.85	−7.77	−4.89	−3.36	−11.96	−9.13	−7.27	+1.99	+0.96	−21.41	−20.46	−13.83	+20.51	+21.69	−38.70
BB1K/MG3S	−12.43	−9.37	−6.15	−4.67	−12.51			+0.82	−0.20	−21.67	−20.70	−14.75	+18.27	+19.46	−41.17
MPWB1K/MG3S	−13.12	−10.04	−6.80	−5.33	−12.38	−9.58	−7.54	+0.22	−0.80	−22.39	−21.32	−14.57	+18.26	+19.45	−40.80
MP2/6-31+G(d,p)	−11.63	−10.02	−3.09	−1.48	−14.68	−9.75	−7.88	+5.02	+3.99	−25.02	−24.25	−14.95	+26.71	+28.18	−41.46
PMP2/6-31+G(d,p)	−14.77	−13.17	−6.53	−4.92	−14.77	−9.72	−7.85	+2.87	+1.83	−25.48	−24.71	−15.40	+18.80	+20.26	−42.87
MCG3/3//MPW1K	−16.45	−13.37	−9.85	−8.32	−15.02	−8.51	−6.65	−0.60	−1.62	−25.31	−24.35	−15.02	+14.56	+15.75	−40.94
MCG3/3//BB1K	−16.47	−13.41	−9.84	−8.36	−15.05			−0.48	−1.49	−25.26	−24.28	−16.97	+14.76	+15.95	−41.01
MCG3/3//MPWB1K	−16.42	−13.35	−9.78	−8.30	−15.01	−9.08	−7.03	−0.53	−1.54	−25.27	−24.20	−16.98	+14.72	+15.92	−40.97
MCG3/3//MP2	−16.05	−12.44	−10.27	−8.66	−14.64	−8.78	−6.91	−0.17	−1.19	−24.97	−24.20	−16.74	+14.43	+15.90	−41.63

[a] V_x and $(V_a^G)_x$ are the classical potential energy and the adiabatic depth of stationary point x, respectively; $V_x^{\ddagger}$ and $(V_a^G)_x^{\ddagger}$ are the classical potential energy barrier and the adiabatic potential energy barrier at SP_x, respectively; and ΔV_x is the classical potential energy for the x channel products. All energies are relative to reactants. Frequencies used in the calculations have been scaled. Scale factors for the different methods in parentheses: MPW1K/MG3S (0.9581),[67] BB1K/MG3S (0.9581),[33] MPWB1K/MG3S (0.9581),[34] MP2/6-31+G(d,p) (0.9661).[68]

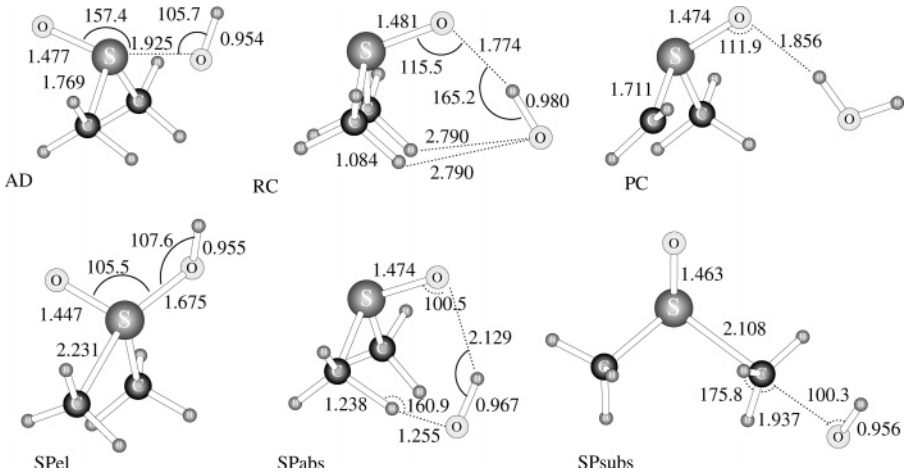

Figure 2. Geometrical representations of the complexes and main saddle points along the three pathways in the DMSO + OH reaction. Distances are given in angstroms and angles in degrees.

Complexes of DMSO with OH. Two types of entrance-channel complexes of DMSO with OH radical were found on the MPW1K/MG3S PES (see Figure 2). On one side, a 2-center−3-electron bond complex (AD) is formed because of the HO−S interaction. Note that the AD structure sligthly deviates from the C_{2v} symmetry (HOSO dihedral angle of −23°). The other complex (RC) has C_{2v} symmetry and is bound between the oxygen atom of DMSO and the hydrogen atom of OH. The AD complex is stabilized by 16.45 kcal/mol with respect to reactants, while the RC structure is only stabilized by 8.51 kcal/mol, both in terms of classical potential energy at the MCG3/3//MPW1K/MG3S level. The binding energies at 0 K (that is, including zero-point energy) of AD and RC are −13.4 and −6.7 kcal/mol, respectively (see Table 1). However, the O−H distance in RC is 1.774 Å, which indicates a relatively strong hydrogen bond. There are two other hydrogen bonds in this structure between the O atom in OH and the H atom in DMSO, but they are much weaker, as can be seen by the corresponding bond distances of 2.790 Å. In agreement with Whang and Zhang results[24] at the MP2/6-311G(d,p) level, but in contrast with Resende et al.[25] calculations at the UMP2/6-31G(d) level, we did not locate a nonsymmetric hydrogen-bonded complex in the entrance channel. Moreover, we found that the H-abstraction saddle-point structure (SP_{abs}) was connected on the PES with the C_{2v} RC structure, being confirmed then as the entrance complex of the R2 channel at the MPW1K/MG3S level. Resende et al.[25] found a different SP_{abs} structure connected with their nonsymmetric entrance-channel complex, whereas Whang an Zhang[24] could not find a path connecting their RC and SP_{abs} structures. The differences between our H-abstraction pathway and that of Resende et al.[25] arise from the position of the abstracted H atom, which is alternated to the S atom in the MPW1K pathway calculated in this work, whereas it is eclipsed to the S atom in Resende's study.

On the other hand, the AD structure at the MPW1K/MG3S level was connected with SP_{el}, which assured that AD was the entrance complex preceding the CH_3 elimination process of the R1 channel, this time in agreement with the two previous theoretical studies using MP2 optimizations.[24,25] In comparison with our previous results[65] at the MCG3/3//MPW1K/MG3S level on the AD complex of the CH_3SCH_3 (DMS) + OH reaction, the S−OH interaction at the AD complex is stronger

TABLE 2: MPW1K/MG3S (low-level) and MCG3/3//MPW1K/MG3S (high-level) Energies (in kcal/mol) for the Different Regions Described in the DMSO + OH Reaction[a]

	ΔV	ΔV_a^G	V ($s=0$)	V_a^G ($s=0$)	$s(V_{max})$	V_{max}	$V_a^G(V_{max})$	$s(V^{AG})$	V^{AG}
				MPW1K/MG3S					
addition	−10.85	−7.77	−1.92	−1.95				+0.307	−1.81
elimination	−11.96	−13.06	−4.89	−3.34				−0.24	−3.27
association	−9.13	−7.27							
abstraction	−13.83	−14.57	+2.00	+0.98				+0.007	+0.98
dissociation	−21.41	−20.46							
S_N2	−38.70	−36.49	+20.51	+21.70				−0.03	+21.71
				MCG3/3//MPW1K/MG3S					
addition	−16.45	−13.37	−2.41	−2.44	0.02	−2.41	−2.43	−0.90	−2.16
elimination	−15.02	−16.13	−9.85	−8.32	+0.18	−9.82	−8.36	−0.07	−8.30
association	−8.51	−6.65							
abstraction	−15.02	−15.76	−0.60	−1.62	−0.12	−0.08	−0.85	−0.27	−0.29
dissociation	−25.31	−24.35							
S_N2	−40.94	−38.73	+14.56	+15.75	+0.20	+15.18	+16.23	+0.18	+16.23

[a] From left to right: classical potential energy and adiabatic energy of reaction for the region; classical potential energy and adiabatic energy at the MPW1K saddle point structure; *s* value at the classical potential energy maximum (on the HL surface); MCG3/3 classical barrier height and adiabatic energy at the classical potential energy maximum; *s* value at the adiabatic energy maximum; adiabatic energy barrier height. All energies relative to reactants (DMSO + OH). The *s* values are in bohr. Zero-point energies (MPW1K/MG3S) are scaled (scale factor = 0.9581).[67]

in the present DMSO + OH system (binding energies at 0 K of −9.5 and −13.4 kcal/mol, respectively), and the S−O bond length is clearly shorter (3.331 vs 1.925 Å).

Saddle-Point Structures of the DMSO + OH Reaction. Three different saddle-point structures were characterized as corresponding to the three main channels in the DMSO + OH reaction. Moreover, a fourth saddle point was located in the addition pathway that leads to the AD complex. In contrast, the association process to form the RC complex was characterized by a continuous decrease of the classical and adiabatic potential energy, that is, it represents a downhill association reaction. The main three saddle-point structures are depicted in Figure 2 as SP_{el}, SP_{abs}, and SP_{subs}. The saddle point found in the addition process is characterized by a very small negative eigenvalue whose associated eigenvector involves the rotation of the OH radical in this region from a long-range OH−S interaction to the short-range HO−S interaction of the AD complex. The OH−S distance takes a value of 3.8 Å at the addition saddle-point structure while the HO−S distance is 3.5 Å. This result is in agreement with our calculations for the addition pathway of the DMS + OH reaction,[65] but none of the previous theoretical works on the DMSO + OH reaction explored the corresponding addition region. Energetically, this saddle point structure lies 2.44 kcal/mol below reactants at the MCG3/3//MPW1K/MG3S level at 0 K (see Table 2). The SP_{el} structure connects the addition complex AD with the elimination products (MSIA, CH_3SOOH and CH_3). It is 8.32 kcal/mol below reactants at 0 K but 5.9 kcal/mol above the AD complex at the MCG3/3//MPW1K/MG3S level. SP_{el} is characterized by a long bond distance between the S atom and the departing methyl group (0.462 Å larger than the corresponding bond in AD). Contrarily, the forming bond is only 0.25 Å shorter than the equilibrium distance of 1.925 Å in AD. SP_{abs} corresponds to the maximum classical potential energy structure along the abstraction pathway. This saddle point connects two complexes: the RC and the PC described previously. The product complex is stabilized by different hydrogen bonds between the forming CH_3SOCH_2 and H_2O products (see Figure 2). This is a difference with the previous theoretical works on this reaction[24,25] where SP_{abs} had been directly linked along the H-abstraction pathway with the abstraction products. On the MCG3/3//MPW1K/MG3S PES explored in our study, PC is stabilized by 8.6 kcal/mol at 0 K with respect to the final products. SP_{abs} is 0.98 kcal/mol above the reactants at the MPW1K level, but after the high-level energy correction, it lies 1.62 kcal/mol below the reactants (always at 0 K). This seems to be a rather surprising result, because there is no experimental evidence of the abstraction products in the DMSO + OH experimental measurements. Finally, SP_{subs} corresponds to the saddle-point structure of the reaction between DMSO and OH to form methanol and the CH_3SO radical. Neither a reactant nor a product complex were found along the substitution pathway, which means that SP_{subs} was directly linked with reactants on one side and with products on the other one. Despite its high exothermicity (more than 40 kcal/mol at 0 K), the adiabatic barrier (15.75 kcal/mol) is higher than for the other two channels. For this reason, the S_N2 channel will not significantly affect the global reaction constant of the DMSO + OH reaction.

3.2. Individual Reaction Channels. In this section, we will analyze the most relevant features of each individual channel: The main characteristics of the reaction pathway will be described for each channel, and the corresponding individual rate constants values will be given and discussed within the CUS formalism,[26] that is, considering that the supermolecules of the reacting system maintain the Boltzmann distribution of energetic states of the bimolecular reactants DMSO + OH along the reaction pathway. In Table 2, the most significant energetic results for all the regions identified in the DMSO + OH reaction pathways are given at the two levels of theory used: the MPW1K/MG3S for low-level and the MCG3/3//MPW1K/MG3S for high-level calculations. In Tables 3 and 4, the rate constants at the low-pressure limit are presented as a function of temperature for R1 and R2 channels, respectively.

MSIA Formation Channel (R1). As has already been mentioned, and was also found in two other previous theoretical works,[24,25] the reaction channel that leads to MSIA formation and CH_3 elimination takes place through the formation of a complex in the entrance channel (denoted AD in this paper). In this way, two distinct regions can be distinguished along the R1 pathway: an addition process from reactants to AD and the elimination region from AD to the final elimination products.

As indicated above, a saddle-point structure was located in the addition pathway, but because of the low value of the imaginary frequency associated to the transition vector, the calculation of the MEP in this region presented several numerical

TABLE 3: Rate Constants (in cm^3 molecule^{-1} s^{-1}) for R1 Channel Computed at the MCG3/3//MPW1K/MG3S Level of Theory at Low-Pressure Limit

	addition		elimination		R1 rate constant
T (K)	$k^{TST}(T)$	$k^{CVT}(T)$	$k^{TST}(T)$	$k^{CVT}(T)$	$k^{CUS}(T)$
200.00	2.87×10^{-10}	9.81×10^{-11}	2.80×10^{-04}	2.10×10^{-04}	9.81×10^{-11}
225.00	1.63×10^{-10}	5.52×10^{-11}	2.66×10^{-05}	2.00×10^{-05}	5.52×10^{-11}
250.00	1.06×10^{-10}	3.55×10^{-11}	4.10×10^{-06}	3.10×10^{-06}	3.55×10^{-11}
298.15	6.01×10^{-11}	1.95×10^{-11}	2.82×10^{-07}	2.12×10^{-07}	1.95×10^{-11}
325.00	4.83×10^{-11}	1.54×10^{-11}	9.13×10^{-08}	6.84×10^{-08}	1.54×10^{-11}
350.00	4.12×10^{-11}	1.30×10^{-11}	3.78×10^{-08}	2.82×10^{-08}	1.30×10^{-11}
375.00	3.63×10^{-11}	1.12×10^{-11}	1.78×10^{-08}	1.32×10^{-08}	1.12×10^{-11}
400.00	3.29×10^{-11}	1.00×10^{-11}	9.26×10^{-09}	6.81×10^{-09}	9.99×10^{-12}
450.00	2.85×10^{-11}	8.46×10^{-12}	3.21×10^{-09}	2.32×10^{-09}	8.43×10^{-12}
500.00	2.61×10^{-11}	7.56×10^{-12}	1.41×10^{-09}	1.00×10^{-09}	7.50×10^{-12}

TABLE 4: Rate Constants (in cm^3 molecule^{-1} s^{-1}) for R2 Channel Computed at the MCG3/3//MPW1K/MG3S Level of Theory at Low-Pressure Limit

	association	abstraction		R2 rate constant
T (K)	$k^{CVT}(T)$	$k^{TST}(T)$	$k^{CVT}(T)$	$k^{CUS}(T)$
200.00	3.06×10^{-08}	1.66×10^{-11}	6.23×10^{-13}	6.23×10^{-13}
225.00	1.20×10^{-08}	9.42×10^{-12}	5.78×10^{-13}	5.78×10^{-13}
250.00	5.83×10^{-09}	6.04×10^{-12}	5.50×10^{-13}	5.50×10^{-13}
298.15	2.16×10^{-09}	3.25×10^{-12}	5.02×10^{-13}	5.02×10^{-13}
325.00	1.45×10^{-09}	2.53×10^{-12}	4.82×10^{-13}	4.82×10^{-13}
350.00	1.07×10^{-09}	2.09×10^{-12}	4.71×10^{-13}	4.71×10^{-13}
375.00	8.31×10^{-10}	1.79×10^{-12}	4.65×10^{-13}	4.65×10^{-13}
400.00	6.38×10^{-10}	1.58×10^{-12}	4.63×10^{-13}	4.63×10^{-13}
450.00	4.21×10^{-10}	1.31×10^{-12}	4.69×10^{-13}	4.68×10^{-13}
500.00	3.10×10^{-10}	1.16×10^{-12}	4.85×10^{-13}	4.84×10^{-13}

problems at some points, and then, we decided to construct a DCP instead. It is important to point out that the existence or not of this saddle point in this region is not kinetically relevant. As will be shown later on, the dynamical bottleneck (under the variational transition-state formalism) of the addition process is due to entropic effects. The selected reaction coordinate was the internuclear distance between the S atom in the DMSO and the O atom of the hydroxyl radical. Along this path, the MCG3/3 classical barrier is negative (−2.41 kcal/mol). Since the MEP was not calculated for this region, the RODS algorithm[48] was essential to obtain reliable generalized eigenvectors and frequencies within the harmonic approximation along the DCP path. However, we found that the directly calculated frequencies of the lowest real frequency modes were not stable or not accurate enough along the reaction path, and this could cause problems in evaluating the zero-point energies and partition functions. On the other hand, the analysis of the generalized eigenvectors associated to the lowest frequencies, revealed that they correspond to rotations of the OH radical, but very coupled with bending movements in the DMSO molecule, rather than corresponding to pure internal rotations of the OH radical. For this reason, a hindered partition function could not be used to improve the harmonic approximation on those modes. To ameliorate this problem, we used the IVTST0-for-frequencies scheme[66] to evaluate the two lowest generalized frequencies along the addition pathway. This scheme is an interpolating procedure which only uses the frequency values at three stationary points (reactants or reactant complex, saddle point, and products or product complex) to describe the evolution of zero-point energy effects along the DCP. After correction for zero-point energies, the adiabatic barrier at the MCG3/3 level is −2.16 kcal/mol, and it is located somewhat closer to the reactants than the saddle point.

In the elimination region, the MEP could be calculated from SP_{el} to AD on one side of the path and to the elimination products (MSIA + CH_3) on the other side. The classical barrier at the MCG3/3 level is −9.82 kcal/mol, and the adiabatic barrier −8.30 kcal/mol. These lower barriers in comparison with the ones at the addition region are the first indication that methyl elimination will be much faster than addition.

When temperature and entropic effects were included along the reaction pathway, the free energy profile was calculated at the different temperatures as a function of s. In Figure 3, the free energy profile at 298.15 K for the complete R1 pathway is presented. The difference between the free energy maxima at the addition and the elimination regions is around 5 kcal/mol. Note that in the addition region there are in fact two free energy maxima separated by a shallow free energy minimum. We mentioned above that, at the addition saddle-point region, the OH fragment is rotating and changing the long-range OH−S interaction with the DMSO fragment by the short-range HO−S interaction. In this range of the reaction pathway, where both interactions are rather loose, several generalized frequencies show a minimum, their entropic contribution to the free energy increases, and consequently, the total free energy in this zone diminishes. The energy difference between the addition and elimination activation free energies could justify that, once the AD complex is formed, it rapidly decomposes by elimination of a methyl group, instead of getting trapped into the AD well and being stabilized by collisions. In fact, there is no experimental evidence of the existence of the AD complex. Urbanski et al.[21] explained that, under the experimental conditions used (at 20 Torr and 298 K), the CH_3 appearance rate was limited by the OH + DMSO addition reaction and not adduct decomposition, and from their measurements, a estimation of the true adduct lifetime would be significantly less than 10 μs. Kukui et al.[23] also analyzed (at 200 and 400 Torr and at 298 K) the possibility of a complex formation followed by its

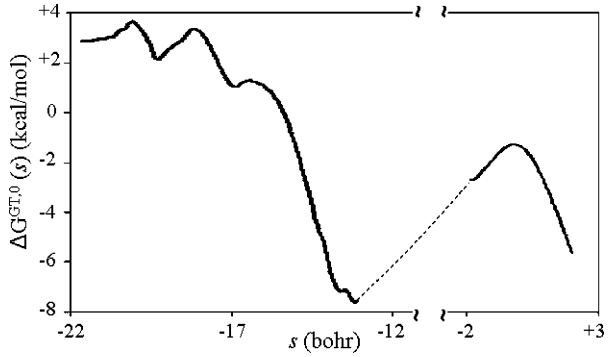

Figure 3. Generalized Gibbs free energy profile at 298.15 K for R1 channel at the MCG3/3//MPW1K/MG3S level. The solid line stands for the calculated pathway, while the dotted line corresponds to the interval of s not calculated. The s values along the addition DCP pathway were calculated with reference to the elimination saddle point ($s = 0$). Note that at $s = -17$ bohr, the HO−S an OH−S distances are 3.3 Å and 2.4 Å, respectively.

reaction with OH and with O_2. No signals of those two reactions were observed. However, Kukui et al.[23] stated that the formation of a short-lived stabilized complex could not be excluded. In any case, the AD stabilization in the DMSO + OH reaction would be less important than for the adduct in the DMS + OH reaction. These results are confirmed in our work: The decomposition adiabatic barrier calculated from the AD minimum to give the elimination products is of only 6.6 kcal/mol compared with the same barrier for the adduct in the DMS + OH reaction of 22 kcal/mol.[65]

In Table 3, the rate constants at each region (addition and elimination) are given as a function of temperature with respect to DMSO + OH as reactants. The symmetry number for the addition proces is 1, while it is 2 for the elimination region because of the existence of two different, but kinetically equivalent, elimination transition states. Note that σ^R and σ^{GT} are equal to 1 in both cases. All those rate constants are calculated within the TST and CVT formalism, but no tunneling corrections were needed, because in both regions, the adiabatic barrier is negative. In the calculation of the CVT addition rate constant, only the highest generalized activation free energy value was considered. The overall R1 rate constants calculated in accordance with CUS theory[26] (as described in eq 2) are also given. The term corresponding to the contribution of the reactive flux at the reactant complex AD is considered negligible, because $k_{AD}(T)$ is much bigger than the addition and elimination rate constants at all temperatures considered.

From the figures in Table 3, it can be observed that both sets of rate constants show some variational effect and a negative temperature dependence. The comparison between the addition and elimination rate constants show clearly that the addition is the dynamical bottleneck of the R1 channel at the whole range of temperatures: Once the complex is formed, it dissociates very easily to form the corresponding products.

Abstraction Channel (R2). No experimental studies have been performed to specifically study the abstraction channel in the DMSO + OH reaction. Urbanski et al.[21] indicated that the unit yield of methyl in their study was consistent with the findings of Hynes and Wine[18] who did not observe a kinetic isotope effect when using deuterated DMSO, and both experiments were showing that the DMSO + OH reaction does not proceed by H-abstraction to any significant extent. Also, Arsene et al.[22] considered this channel to be of minor significance, since there was no indication for primary formation of SO_2. In our theoretical calculations, the R2 mechanism was found to proceed via a complex in the entrance channel (RC), a saddle-point structure (SP_{abs}), and another complex at the product side (PC). The connection between SP_{abs}, RC, and PC had not been proven before. We already mentioned that Whang and Zhang[24] did not ensure the connection between RC and SP_{abs} and that Resende et al.[25] explored a different H-abstraction pathway. Three distinct regions can be distinguished then along the R2 channel: an association region from reactants to RC, the abstraction region from RC to PC, and a dissociation region from PC to the final abstraction products. The same stationary points along the H-abstraction pathway were found for the DMS + OH reaction.[65]

The association process to form RC is a downhill reaction without a saddle point, so we constructed a DCP path using the O−H internuclear distance between the O atom in DMSO and the hydrogen atom in OH as the reaction coordinate, while the other degrees of freedom were allowed to relax. Only when the free energy is evaluated along the DCP does a maximum appear, so that the variational transition-state rate constant can be calculated for this association.

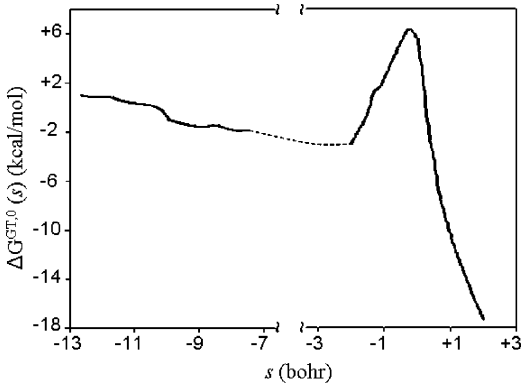

Figure 4. Generalized Gibbs free energy profile at 298.15 K for R2 channel at the MCG3/3//MPW1K/MG3S level. The solid line stands for the calculated pathway, while the dotted line corresponds to the interval of *s* not calculated. The *s* values along the association DCP pathway were calculated with reference to the abstraction saddle point ($s = 0$).

In the abstraction region, the MEP could be calculated from SP_{abs} down to RC on the reactant side of the path and down to PC on the product side. The classical barrier at the MCG3 level is slightly negative: −0.08 kcal/mol. When the harmonic generalized frequencies along the MEP were analyzed, we detected that the lowest real one was unstable (became imaginary) in several regions along the MEP at the product side. The analysis of the generalized eigenvector associated to this lowest frequency revealed that it did not correspond to an internal rotation of the OH radical. For this reason, a hindered partition function could not be used to improve the harmonic approximation on that mode. We then decided that the more physical description for the evolution of this frequency along the reaction pathway would result from the three-point interpolation IVTST0-for-frequencies scheme[66] described in the previous section. In this way, an adiabatic energy profile could be constructed that presents an adiabatic barrier of −0.29 kcal/mol. This result indicates that at 0 K the H-abstraction process would not really be impeded, although the adiabatic barriers encountered for the addition and elimination bottlenecks of the R1 channel are still more negative.

When the partition functions were obtained along the reaction pathway, the free energy profile was calculated at the different temperatures as a function of *s*. In Figure 4, the free energy profile at 298.15 K for the complete R2 pathway is depicted. We can see from this figure that the dynamical bottleneck of the R2 channel is located at the H-abstraction region. The high generalized activation free energy at the H-abstraction transition state is due to entropic constraints imposed for such tight structure.

In Table 4, the rate constants at each region (association and abstraction) are given as a function of temperature with respect to DMSO + OH as reactants. Recall that the dissociation region was not considered in the rate constant calculation. The symmetry number for the association process is 1, while it is 2 for the abstraction region because of the existence of two different, but kinetically equivalent, abstraction transition states. Note that σ^R and σ^{GT} are 1 in both cases. The association rate constants could only be calculated within the CVT formalism, because it is a process without a saddle point, while for the abstraction process, the TST and CVT rate constants were calculated. No tunneling corrections were needed, because in both regions, the adiabatic barrier is negative.

TABLE 5: Rate Constants (in cm^3 molecule^{-1} s^{-1} for the DMSO + OH Reaction Computed at the MCG3/3//MPW1K/MG3S Level of Theory at Low-Pressure Limit

T (K)	$k_{R1}(T)$	$k_{R2}(T)$	$k_{R3}(T)$	$k^{CCUS}(T)$
200.00	9.81×10^{-11}	6.23×10^{-13}	7.65×10^{-27}	9.87×10^{-11}
225.00	5.52×10^{-11}	5.78×10^{-13}	1.69×10^{-26}	5.58×10^{-11}
250.00	3.55×10^{-11}	5.50×10^{-13}	9.11×10^{-26}	3.60×10^{-11}
298.15	1.95×10^{-11}	5.02×10^{-13}	5.95×10^{-24}	2.00×10^{-11}
325.00	1.54×10^{-11}	4.82×10^{-13}	4.60×10^{-23}	1.59×10^{-11}
350.00	1.30×10^{-11}	4.71×10^{-13}	2.47×10^{-22}	1.35×10^{-11}
375.00	1.12×10^{-11}	4.65×10^{-13}	1.09×10^{-21}	1.17×10^{-11}
400.00	9.99×10^{-12}	4.63×10^{-13}	4.12×10^{-21}	1.04×10^{-11}
450.00	8.43×10^{-12}	4.68×10^{-13}	3.96×10^{-20}	8.90×10^{-12}
500.00	7.50×10^{-12}	4.84×10^{-13}	2.54×10^{-19}	7.99×10^{-12}

It must be remarked that the association rate constant values presented in Table 4 might be somewhat overestimated in the range from 200 to 350 K, because the free energy maximum could not be located in the calculated association reaction pathway. In any case, the comparison between the association and abstraction rate constants show clearly that the abstraction is the dynamical bottleneck of the R2 channel. Concerning the abstraction rate constant, a significant variational effect is observed. In accordance with the abstraction rate constant contribution, the R2 rate constant presents a slightly negative temperature dependence that begins to invert above 450 K.

Methanol Formation Channel (R3). As indicated before, the reaction pathway of the R3 channel presents only one region corresponding to the substitution region like in the DMS + OH reaction.[65] This way, the MEP was constructed from SP_{subs} down to reactants and products, as no complexes were found either in the entrance or in the exit channels. The classical barrier at the MCG3/3 level and the adiabatic barrier are 15.8 and 16.3 kcal/mol, respectively. The free energy barrier at 298.15 K is 22.3 kcal/mol, clearly higher than for the other two channels. The symmetry number used in the rate constant calculation is 2, because there are two kinetically equivalent transition states. As expected, because of the high classical potential energy barrier, the variational effects are small in this process, but tunneling effects cannot be obviated. At 298.15 K, for instance, the $k^{TST} = 6.17 \times 10^{-25}$, while the $k^{CVT} = 6.01 \times 10^{-25}$, and $k^{CVT/SCT} = 2.65 \times 10^{-24}$ cm^3 molecule^{-1} s^{-1}. These rate constant values confirm that the R3 channel is not kinetically relevant in the degradation process of DMSO + OH.

3.3. Overall DMSO + OH Rate Constant. Once we calculated the rate constants for each one of the three possible pathways identified for the DMSO + OH reaction, they were combined as competitive mechanisms following the CCUS theory expressed in eq 1. The results are shown in Table 5. These final figures at the low-pressure regime verify that the addition−elimination channel (and, specifically, the addition process that leads to the AD adduct) is the dominant channel in the global degradation mechanism of DMSO by OH. The branching ratios at 298.15 K are the following: 97.5% for the addition−elimination, 2.5% for the abstraction, and 0 for the S_N2 process. These results are in agreement with experimental measurements, although we might be seeing a more important contribution of the abstraction channel. In addition, as the R1 rate constant diminishes when temperature is increased more rapidly than the R2 rate constant, the abstraction branching ratio increases at higher temperatures (for instance, its value at 500 K is already 6.1%). In Figure 5, the Arrhenius plots for the R1, R2, and global rate constants are shown. In comparison with the experimental values for the overall rate constant (only carried out at 298 K), which range from $(5.9 \pm 1.5) \times 10^{-11}$ to $(9 \pm 2) \times 10^{-11}$ cm^3 molecule^{-1} s^{-1}, our calculated value of 2.00×10^{-11} cm^3 molecule^{-1} s^{-1} may seem somewhat low. It has to be taken into acount, though, that a difference of only 1 kcal/mol (amount that is often considered the limit of chemical accuracy) in the free energy values already represents a factor of 3 in the rate constant (compare, for example, the TST and CVT rate constants at 298.15 K for the addition process in Table 3, which present such a difference in their corresponding generalized activation Gibbs free energies). In addition, as it was not clear experimentally whether the AD adduct is really a stabilized intermediate in the DMSO + OH reaction, and also because the only previous calculated rate constants for this process had been obtained by assuming the equilibration of the entrance-channel complexes, we decided to recalculate the overall rate constants simulating a high enough pressure regime. In this calculation, it was considered that the reacting supermolecules acquire the Boltzmann distribution of energetic states of each complex found along the reaction pathway. The one-way flux rate constants of R1 and R2 channels were calculated according to eqs 6 and 7, where the steady-state approximation was used and AD and RC were taken as short-lived thermalized complexes. The final results for the overall rate constant as a function of temperature are shown in Table 6. The overall high-pressure rate constant values are very similar to the corresponding values within the CCUS formulation (see Table 5). This result would be in agreement with the experimental studies where no pressure dependence of the rate constant was detected. In fact, the calculated high-pressure rate constants are slightly greater than the low-pressure ones. This difference does not come, though, from the R1 rate constants but from the R2 channel. The $k_{abs}^{High-P}(T)$ (in eq 7) takes bigger values than $k_{abs}(T)$ (in eq 3), although the energy barrier is higher in the first case, because the high-pressure rate constant is corrected by a tunneling transmission factor greater than 1, whereas there is no tunneling at the abstraction bottleneck in the low-pressure

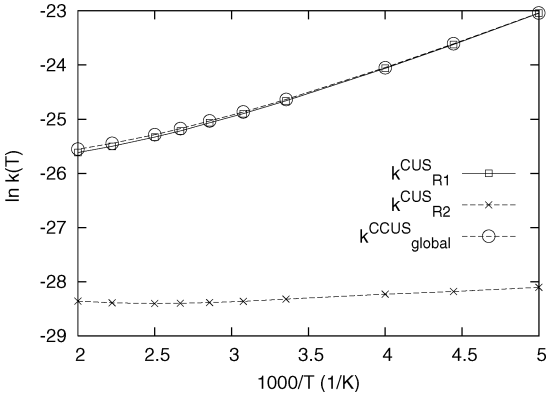

Figure 5. Arrhenius plot for the addition−elimination (R1), abstraction (R2), and global rate constants of the DMSO + OH reaction at the low-pressure regime.

TABLE 6: Rate Constants (in cm^3 molecule^{-1} s^{-1}) for the DMSO + OH Reaction Computed at the MCG3/3//MPW1K/MG3S Level of Theory at High-Pressure Limit

T (K)	$k_{R1}(T)$	$k_{R2}(T)$	$k_{R3}(T)$	$k^{High-P}(T)$
200.00	9.81×10^{-11}	6.09×10^{-11}	7.65×10^{-27}	1.59×10^{-10}
225.00	5.52×10^{-11}	2.10×10^{-11}	1.69×10^{-26}	7.61×10^{-11}
250.00	3.55×10^{-11}	9.70×10^{-12}	9.11×10^{-26}	4.52×10^{-11}
298.15	1.95×10^{-11}	3.56×10^{-12}	5.95×10^{-24}	2.31×10^{-11}
325.00	1.54×10^{-11}	2.42×10^{-12}	4.60×10^{-23}	1.79×10^{-11}
350.00	1.30×10^{-11}	1.82×10^{-12}	2.47×10^{-22}	1.48×10^{-11}
375.00	1.12×10^{-11}	1.44×10^{-12}	1.09×10^{-21}	1.27×10^{-11}
400.00	1.00×10^{-11}	1.19×10^{-12}	4.12×10^{-21}	1.12×10^{-11}
450.00	8.43×10^{-12}	7.58×10^{-12}	3.96×10^{-20}	9.19×10^{-12}
500.00	7.51×10^{-12}	6.31×10^{-13}	2.54×10^{-19}	8.14×10^{-12}

limit. In comparison with the result of Resende et al.[25] at 298 K for the high-pressure global rate constant (1.44×10^{-10} cm^3 molecule^{-1} s^{-1}), our calculated value of 2.31×10^{-11} cm^3 molecule^{-1} s^{-1} is nearly 1 order of magnitude lower. However, it can be observed from the figures in Table 6 that the overall rate constant increases very rapidly with decreasing temperature. At 200 K, for instance, its value is already 1.59×10^{-10} cm^3 molecule^{-1} s^{-1}.

4. Conclusions

In this study, the overall rate constant for the DMSO + OH reaction was calculated within the framework of variational transition-state theory, including tunneling corrections when needed. In agreement with previous experimental and theoretical studies, three distinct reaction channels were characterized: an addition−elimination channel (R1) that leads to MSIA formation and CH_3 elimination, an abstraction channel (R2) that leads to CH_3SOCH_2 formation, and an S_N2-type channel (R3) that leads to methanol formation. The S_N2-type pathway presents a very high free energy barrier and is not kinetically competitive. The addition−elimination channel is the most kinetically relevant. Along this pathway, two regions can be distinguished: the addition region where an entrance-channel adduct (AD) is formed, stabilized by a 2-center−3-electron HO−S interaction, and an elimination region that leads to the elimination products via a saddle point. Both processes take place with negative adiabatic barriers, but entropic effects make the addition step the determinant bottleneck of the R1 channel. The abstraction channel takes place via an entrance channel complex (RC) stabilized by a dipole−dipole OH−OS interaction followed by a H-abstraction saddle point. Entropic constraints make the abstraction transition state the determinant bottleneck of the R2 channel. The rate constants for each individual kinetic channel were calculated with the use of CUS theory that computes the one-way flux along a particular pathway in the low-pressure limit. The global rate constant was obtained with the CCUS formalism that takes into account competitive kinetic channels in the evaluation of the global flux. The overall rate constant at 298.15 K is 2.0×10^{-11} cm^3 molecule^{-1} s^{-1}, and it is determined by the free energy barrier in the formation of the AD adduct. Our main point here is that this AD free energy barrier, in the temperature range analyzed in our study, corresponds to the inner transition state of the adduct formation, because it is located in that region where chemical interactions are of similar, or somewhat greater, strength than the long-range interactions. This bottleneck is completely different than the one associated with the formation of the RC complex and cannot be calculated with long-range expressions based on collisional models as has been previously done. The abstraction channel is not competitive at 298.15 K, but its branching ratio increases with temperature. Calculations carried out using a high-pressure formulation gave the same results for the overall rate constants as a function of temperature, in good agreement with experimental data, which had not shown pressure dependence of the DMSO degradation reaction by OH.

Acknowledgment. We are grateful for financial support from the Spanish "Ministerio de Ciencia y Tecnología" and the "Fondo Europeo de Desarrollo Regional" through project no. BQU2002-00301 and the use of the computational facilities of the CESCA. We would like to acknowlege Prof. K. V. Mikkelsen and Dr. A. Gross from University of Copenhagen for nice discussion and ideas. N.G.-G. also acknowledges the "Generalitat de Catalunya" for the FI Grant.

References and Notes

(1) Barnes, I.; Becker, K. H.; Patroescu, I. *Geophys. Res. Lett.* **1994**, *21*, 2389.
(2) Barnes, I.; Becker, K. H.; Patroescu, I. *Atmos. Environ.* **1996**, *30*, 1805.
(3) Sørensen, S. S.; Falbe-Hansen, H.; Mangoni, M.; Hjorth, J.; Jensen, N. R. *J. Atmos. Chem.* **1996**, *24*, 299.
(4) Arsene, C.; Barnes, I.; Becker, K. H. *Phys. Chem. Chem. Phys.* **1999**, *1*, 5463.
(5) Arsene, C.; Barnes, I.; Becker, K. H.; Mocanu, R. *Atmos. Environ.* **2001**, *35*, 3769.
(6) Bandy, A.; Thornton, D.; Blomquist, B.; Chen, S.; Wade, T.; Ianni, J.; Mitchell, G.; Nadler, W. *Geophys. Res. Lett.* **1996**, *23*, 741.
(7) Berresheim, H.; Huey, J.; Thorn, R.; Eisele, F.; Tanner, D.; Jefferson, A. *J. Geophys. Res.* **1998**, *103*, 1629.
(8) Sciare, J.; Baboukas, E.; Hancy, R.; Mihalopoulos, N.; Nguyen, B. *J. Atmos. Chem.* **1998**, *30*, 229.
(9) Andreae, M. *Marine Chem.* **1990**, *30*, 1.
(10) Spiro, P.; Jacob, D.; Logan, J. *J. Geophys. Res.* **1992**, *97*, 6023.
(11) Bates, T. S.; Lamb, B. K.; Guenther, A.; Dignon, J.; Stoiber, R. E. *J. Atmos. Chem.* **1992**, *14*, 315.
(12) Charlson, R. J.; Lovelock, J. E.; Andreae, M. O.; Warren, S. G. *Nature (London)* **1987**, *326*, 655.
(13) Arsene, C.; Barnes, I.; Becker, K. H.; Mocanu, R. *Atmos. Environ.* **2001**, *35*, 3769.
(14) Turnipseed, A. A.; Barone, S. B.; Ravishankara, A. R. *J. Phys. Chem.* **1996**, *100*, 14703.
(15) Barnes, I.; Bastian, V.; Becker, K.; Overath, R. *Int. J. Chem. Kinet.* **1991**, *23*, 579.
(16) Toumi, R. *Geophys. Res. Lett.* **1994**, *21*, 117.
(17) Ingham, T.; Bauer, D.; Sander, R.; Crutzen, P.; Crowley, J. *J. Phys. Chem. A* **1999**, *103*, 7199.
(18) Hynes, A.; Wine, P. *J. Atmos. Chem.* **1996**, *24*, 23.
(19) Williams, M. B.; Campuzano-Jost, P.; Bauer, D.; Hynes, A. J. *Chem. Phys. Lett.* **2001**, *344*, 61.
(20) Barnes, I.; Bastian, V.; Becker, K.; Martin, D. *Biogenic Sulfur in the Environment*; Saltzman, E. S., Cooper, W. J., Eds.; ACS Symposium Series 393; American Chemical Society: Washington, DC, 1989; pp 476−488.
(21) Urbanski, S.; Stickel, R.; Wine, P. *J. Phys. Chem. A* **1998**, *102*, 10522.
(22) Arsene, C.; Barnes, I.; Becker, K.; Schneider, W.; Wallington, T.; Mihalopoulos, N.; Patroescu-Klotz, I. *Environ. Sci. Technol.* **2002**, *36*, 5155.
(23) Kukui, A.; Borissenko, D.; Laverdet, G.; Bras, G. L. *J. Phys. Chem. A* **2003**, *107*, 5732.
(24) Wang, L.; Zhang, J. *Chem. Phys. Lett.* **2002**, *356*, 490.
(25) Resende, S. M.; de Bona, J. C.; de Souza, P. *Chem. Phys.* **2005**, *309*, 283.
(26) Hu, W.-P.; Truhlar, D. G. *J. Am. Chem. Soc.* **1995**, *117*, 10726.
(27) Møller, C. M.; Plesset, M. S. *Phys. Rev.* **1934**, *46*, 618.
(28) Becke, A. D. *J. Chem. Phys.* **1993**, *98*, 5648.
(29) Gunnarsson, O.; Lundqvist, B. I. *Phys. Rev. B* **1976**, *13*, 4274.
(30) Langreth, D. C.; Perdew, J. P. *Phys. Rev. B* **1977**, *15*, 2884.
(31) Kohn, W.; Becke, A. D.; Parr, R. G. *J. Phys. Chem.* **1996**, *100*, 12974.
(32) Lynch, J.; Fast, P. L.; Harris, M.; Truhlar, D. G. *J. Phys. Chem. A* **2000**, *104*, 4812.
(33) Zhao, Y.; Lynch, B. J.; Truhlar, D. G. *J. Phys. Chem. A* **2004**, *108*, 2715.
(34) Zhao, Y.; Truhlar, D. G. *J. Phys. Chem. A* **2004**, *108*, 6908.
(35) Perdew, J. P. *Electronic Structure of Solids '91*; Ziesche, P., Eschig, H., Eds.; Akademie Verlag: Berlin, 1991; p 11.
(36) Becke, A. D. *J. Chem. Phys.* **1996**, *104*, 1040.
(37) Perdew, J. P. *Phys. Rev. Lett.* **1985**, *55*, 1665.
(38) Zhao, Y.; González-García, N.; Truhlar, D. G. *J. Phys. Chem. A* **2005**, *109*, 2012.
(39) Schlegel, H. B. *J. Phys. Chem.* **1988**, *92*, 3075.
(40) Hehre, W. J.; Radom, L.; Schleyer, P. V. R.; Pople, J. A. *Ab Initio Molecular Orbital Theory*; Wiley: New York, 1986.
(41) Lynch, B. J.; Zhao, Y.; Truhlar, D. G. *J. Phys. Chem. A* **2003**, *107*, 1384.
(42) Fast, P. L.; Truhlar, D. G. *J. Phys. Chem. A* **2000**, *104*, 6111.
(43) Lynch, B. J.; Truhlar, D. G. *J. Phys. Chem. A* **2002**, *106*, 842.
(44) Lynch, B. J.; Truhlar, D. G. *J. Phys. Chem. A* **2003**, *107*, 3898.
(45) Truhlar, D. G.; Kupperman, A. *J. Am. Chem. Soc.* **1971**, *93*, 1840.
(46) Page, M.; McIver, J. W. *J. Chem. Phys.* **1988**, *88*, 922.
(47) Chuang, Y.-Y.; Corchado, J. C.; Truhlar, D. G. *J. Phys. Chem. A* **1999**, *103*, 1140.
(48) Villà, J.; Truhlar, D. G. *Theor. Chem. Acc.* **1997**, *97*, 317.
(49) Frisch, M. J.; Trucks, G. W.; Schlegel, H. B.; Scuseria, G. E.; Robb, M. A.; Cheeseman, J. R.; Montgomery, J. A., Jr.; Vreven, T.; Kudin, K. N.; Burant, J. C.; Millam, J. M.; Iyengar, S. S.; Tomasi, J.; Barone, V.;

Mennucci, B.; Cossi, M.; Scalmani, G.; Rega, N.; Petersson, G. A.; Nakatsuji, H.; Hada, M.; Ehara, M.; Toyota, K.; Fukuda, R.; Hasegawa, J.; Ishida, M.; Nakajima, T.; Honda, Y.; Kitao, O.; Nakai, H.; Klene, M.; Li, X.; Knox, J. E.; Hratchian, H. P.; Cross, J. B.; Bakken, V.; Adamo, C.; Jaramillo, J.; Gomperts, R.; Stratmann, R. E.; Yazyev, O.; Austin, A. J.; Cammi, R.; Pomelli, C.; Ochterski, J. W.; Ayala, P. Y.; Morokuma, K.; Voth, G. A.; Salvador, P.; Dannenberg, J. J.; Zakrzewski, V. G.; Dapprich, S.; Daniels, A. D.; Strain, M. C.; Farkas, O.; Malick, D. K.; Rabuck, A. D.; Raghavachari, K.; Foresman, J. B.; Ortiz, J. V.; Cui, Q.; Baboul, A. G.; Clifford, S.; Cioslowski, J.; Stefanov, B. B.; Liu, G.; Liashenko, A.; Piskorz, P.; Komaromi, I.; Martin, R. L.; Fox, D. J.; Keith, T.; Al-Laham, M. A.; Peng, C. Y.; Nanayakkara, A.; Challacombe, M.; Gill, P. M. W.; Johnson, B.; Chen, W.; Wong, M. W.; Gonzalez, C.; Pople, J. A. *Gaussian 03*, revision C.02; Gaussian, Inc.: Wallingford, CT, 2004.

(50) Zhao, Y.; Rodgers, J. M.; Lynch, B. J.; Fast, P. L.; Pu, J.; Chuang, Y.-Y.; Truhlar, D. G. *Multilevel*, v. 4.0/G03; University of Minnesota, Minneapolis, MN, 2004; http://comp.chem.umn.edu/multilevel.

(51) Corchado, J. C.; Chuang, Y.-Y.; Coitiño, E. L. C.; Truhlar, D. G. *GaussRate 9.1*; University of Minnesota, Minneapolis, MN, 2003; http://comp.chem.umn.edu/gaussrate.

(52) Corchado, J. C.; Chuang, Y.-Y.; Fast, P. L.; Villà, J.; Hu, W.-P.; Liu, Y.-P.; Lynch, G. C.; Nguyen, K. A.; Jackels, C. F.; Melissas, V. S.; Lynch, B. L.; Rossi, I.; Coitiño, E. L. C.; Fernández-Ramos, A.; Pu, J.; Albu, T. V.; Steckler, R.; Garret, B. C.; Isaacson, A. D.; Truhlar, D. G. *PolyRate 9.3*; University of Minnesota, Minneapolis, MN, 2004; http://comp.chem.umn.edu/polyrate.

(53) Hu, W.-P.; Truhlar, D. G. *J. Am. Chem. Soc.* **1996**, *118*, 860.

(54) Garrett, B. C.; Truhlar, D. G. *J. Chem. Phys.* **1979**, *70*, 1593.

(55) Garrett, B. C.; Truhlar, D. G.; Grev, R. S.; Magnuson, A. W. *J. Phys. Chem.* **1980**, *84*, 1730.

(56) Isaacson, A. D.; Truhlar, D. G. *J. Chem. Phys.* **1982**, *76*, 1380.

(57) Truhlar, D. G.; Isaacson, A. D.; Garrett, B. C. *Theory of Chemical Reaction Dynamics*; CRC Press: Boca Raton, FL, 1985; p 65.

(58) Fernández-Ramos, A.; Miller, J. A.; Klippenstein, S. J.; Truhlar, D. G., *Comprehensive Chemical Kinetics*; Elsevier, to be published.

(59) Liu, Y. P.; Lynch, G. C.; Truong, T. N.; Lu, D. H.; Truhlar, D. G.; Garrett, B. C. *J. Am. Chem. Soc.* **1993**, *115*, 2408.

(60) Lu, D. H.; Truong, T. N.; Melissas, V.; Lynch, G. C.; Liu, Y. P.; Garrett, B. C.; Steckler, R.; Isaacson, A. D.; Rai, S. N.; Hancock, G. C.; Laurderdale, J. G.; Joseph, T.; Truhlar, D. G. *Comput. Phys. Commun.* **1992**, *71*, 235.

(61) Truhlar, D. G.; Gordon, M. S. *Science* **1990**, *249*, 491.

(62) Truong, T. N.; Lu, D. H.; Lynch, G. C.; Liu, Y. P.; Melissas, V.; Stewart, J. J. P.; Steckler, R.; Garrett, B. C.; Isaacson, A. D.; González-Lafont, A.; Rai, S. N.; Hancock, G. C.; Joseph, T.; Truhlar, D. G. *Comput. Phys. Commun.* **1993**, *75*, 143.

(63) Pechukas, P. *J. Chem. Phys.* **1976**, *64*, 1516.

(64) Corchado, J. C.; Coitiño, E. L. C.; Chuang, Y. Y.; Fast, P. L.; Truhlar, D. G. *J. Phys. Chem.* **1998**, *102*, 2424.

(65) González-García, N.; González-Lafont, A.; Lluch, J. M. *J. Comput. Chem.* **2005**, *26*, 569.

(66) Hu, W.; Liu, Y.; Truhlar, D. *Faraday Trans. Chem. Soc.* **1994**, *90*, 1715.

(67) Zhao, Y.; Lynch, B. J.; Truhlar, D. G. *J. Phys. Chem. A* **2004**, *108*, 2715.

(68) Scott, A. P.; Radom, L. *J. Phys. Chem.* **1996**, *100*, 16502.